

Microscopic phase diagram of $\text{Eu}(\text{Fe}_{1-x}\text{Ni}_x)\text{As}_2$ ($x = 0, 0.04$) under pressureWenli Bi ^{1,*}, Zachary Nix ¹, Utpal Dutta,¹ Jiyong Zhao,² Esen E. Alp,² Dongzhou Zhang,³ Paul Chow,⁴ Yuming Xiao,⁴ Ya-Bin Liu,⁵ Guang-Han Cao,⁵ and Yogesh K. Vohra¹¹*Department of Physics, University of Alabama at Birmingham, Birmingham, Alabama 35294, USA*²*Advanced Photon Source, Argonne National Laboratory, Argonne, Illinois 60439, USA*³*Hawaii Institute of Geophysics and Planetology, School of Ocean and Earth Science and Technology, University of Hawaii at Manoa, Honolulu, Hawaii 96822, USA*⁴*HPCAT, X-ray Science Division, Argonne National Laboratory, Argonne, Illinois 60439, USA*⁵*Department of Physics, Zhejiang University, Hangzhou 310027, China*

(Received 22 June 2020; revised 13 December 2020; accepted 4 May 2021; published 17 May 2021)

To establish the microscopic P-T phase diagram of recent 112-type iron-pnictides $\text{Eu}(\text{Fe}_{1-x}\text{Ni}_x)\text{As}_2$ ($x = 0, 0.04$), high-pressure synchrotron Mössbauer spectroscopy experiments in ^{151}Eu and ^{57}Fe have been performed. In EuFeAs_2 application of pressure completely suppresses the itinerant electron magnetism from the Fe sublattice and the local-moment magnetism in Eu ions at ~ 10 and ~ 11.6 GPa, respectively. High-pressure x-ray diffraction experiments in EuFeAs_2 reveal an anomalous change in the lattice parameters and a discontinuity in volume around 10 GPa, suggesting an isostructural transition at this pressure. With Ni-doping ($x = 0.04$), a collapse of local magnetic order occurs at ~ 8 GPa, a lower critical pressure compared with the parent compound. In both systems, the suppression of local-moment magnetism is associated with a significant increase of mean valence in Eu ions.

DOI: [10.1103/PhysRevB.103.195135](https://doi.org/10.1103/PhysRevB.103.195135)**I. INTRODUCTION**

Since the discovery of high-temperature superconductivity at 26 K in $\text{LaFeAsO}_{1-x}\text{F}_x$ [1], a number of iron-based superconductors with various crystal structures have been reported [2–12]. Among these materials, special attention has been paid to iron-pnictides containing Eu in which both Fe and Eu sublattices possess magnetic moment [13–20]. Under pressure or with chemical doping superconductivity emerges and coexists with the strong local-moment magnetism from divalent Eu ions, making these systems a unique platform to investigate the interplay of magnetism and superconductivity. For instance, EuFe_2As_2 , an 122-type pnictide, shows a spin-density-wave (SDW) order near 190 K from the Fe_2As_2 layer and type-A antiferromagnetic order near 20 K from strong localized magnetic moment in the Eu ions [14,17]. The SDW order is accompanied by a tetragonal-to-orthorhombic transition, which can be suppressed via chemical doping or application of external pressure [15,16,21–29]. When this happens, superconductivity emerges below 30 K at a pressure of 2.5–3 GPa and coexists with the local magnetic order from Eu ions [24–26]. Since the superconducting critical temperature (T_C) is higher than the Néel temperature (T_N) of Eu ions which is ~ 20 K in the superconducting pressure regime, it is interesting that in EuFe_2As_2 the electrical resistivity shows a reentrant superconductivity caused by the magnetic ordering of Eu^{2+} moment [27].

Another family of so-called 1144-type tetragonal compounds $\text{AEuFe}_4\text{As}_4$ ($A = \text{Rb}, \text{Cs}$) exhibits a robust coexistence of superconductivity with $T_C \sim 35$ K and ferromagnetism below ~ 15 K from Eu ions at ambient pressure [19,20,30]. Similar to EuFe_2As_2 , reentrant superconductivity has been observed below the Curie temperature. In these systems, with application of pressure magnetic-ordering temperature (T_o) is enhanced while the superconductivity is suppressed [31,32].

Very recently, the discovery of a new 112-type of iron-pnictide EuFeAs_2 has been reported [33,34]. EuFeAs_2 consists of alternately stacked Fe_2As_2 layers and zigzag As-chain layers. It shows two primary magnetic transitions at ~ 106 and ~ 40 K, associated with SDW transition and antiferromagnetic ordering in the Fe and Eu sublattices, respectively [33–35]. La-doping suppresses both magnetic transition temperatures and induces superconductivity [33]. However, Ni-doping suppresses the SDW order only and shows almost no effect on the local magnetic order of Eu. Moreover, 4% Ni-doping suppresses the SDW order completely and induces bulk superconductivity with T_C of 17.5 K [34]. It is interesting that in $\text{Eu}(\text{Fe}_{0.96}\text{Ni}_{0.04})\text{As}_2$ superconductivity occurs at a lower temperature than the Néel temperature of Eu^{2+} ions ($T_C < T_N$), in contrast with the Eu-containing 122- and 1144-type iron pnictide superconductors where $T_C > T_N$.

It is of considerable significance to systematically investigate the complex phase diagram, especially on a microscopic scale, in these representative Eu-based iron-pnictides to construct a generic phase diagram and understand the role of magnetism and its interplay with superconductivity. In an attempt to provide detailed and microscopic information on

*Corresponding author: wbi@uab.edu

magnetism, valence, and evolution of crystal structure in this new family of Fe-pnictide, we have conducted the first high-pressure study in $\text{Eu}(\text{Fe}_{1-x}\text{Ni}_x)\text{As}_2$ ($x = 0, 0.04$) utilizing a combined experimental approach including high-pressure diamond anvil cell, synchrotron Mössbauer spectroscopy (SMS), and x-ray diffraction (XRD). We have found that in the parent compound, EuFeAs_2 , both the local-moment magnetism in Eu ions and the SDW order from Fe sublattice are suppressed by external pressure. Similar to EuFeAs_2 , application of pressure in $\text{Eu}(\text{Fe}_{0.96}\text{Ni}_{0.04})\text{As}_2$ also suppresses the local-moment magnetism. In both systems the collapse of local-moment magnetism is associated with a significant increase of mean valence in Eu ions. XRD experiments in EuFeAs_2 reveal that the ambient orthorhombic structure is maintained up to 22 GPa with an anomaly in the lattice parameters and unit-cell volume around 10 GPa.

II. EXPERIMENTAL METHODS

In this study, polycrystalline samples of $\text{Eu}(\text{Fe}_{1-x}\text{Ni}_x)\text{As}_2$ ($x = 0, 0.04$) were synthesized from solid-state reaction in vacuum as detailed in Ref. [34]. High-pressure SMS experiments in ^{151}Eu and ^{57}Fe were carried out at the 3ID and 16ID-D (HPCAT) Beamlines, respectively, at the Advanced Photon Source (APS), Argonne National Laboratory (ANL). Mössbauer spectroscopy is isotope sensitive and a unique technique to probe the individual magnetism in systems containing multiple magnetic species such as Eu and Fe [29]. Time-domain SMS experiments were carried out at the nuclear resonant energy of 21.54 keV for ^{151}Eu and 14.41 keV for ^{57}Fe isotopes. SMS experiments in both ^{151}Eu and ^{57}Fe isotopes were conducted in EuFeAs_2 to investigate the magnetic transitions in Eu and Fe sublattices, while ^{151}Eu SMS experiments were carried out in $\text{Eu}(\text{Fe}_{0.96}\text{Ni}_{0.04})\text{As}_2$.

High pressures were achieved using a gas membrane-driven miniature diamond anvil cell with one pair of anvils of 500 μm culet for SMS experiment in ^{151}Eu [36] and a symmetric diamond anvil cell with anvils of 400 μm culet driven by a push-pull dual membrane system to maintain constant pressure for a wide temperature range for ^{57}Fe SMS experiment [37]. Re gaskets were preindented to 80 and 77 μm and holes of 250 and 200 μm were drilled to form the sample chambers in DACs with anvils of 500 and 400 μm culets, respectively. The polycrystalline EuFeAs_2 and $\text{Eu}(\text{Fe}_{0.96}\text{Ni}_{0.04})\text{As}_2$ samples were loaded in the sample chambers together with two or three pieces of ruby spheres as *in situ* pressure marker [38]. Neon was used as pressure medium. The valence state of Eu ions was studied by measuring the isomer shift (IS) of ^{151}Eu using a reference sample with known IS value. In this study, trivalent Eu_2O_3 and divalent EuS with IS of 1.024 mm/s and -11.496 mm/s, respectively, relative to EuF_3 [39] were used [40].

The synchrotron x-rays were focused to $15 \times 15 \mu\text{m}$ (FWHM) and $5 \times 5 \mu\text{m}$ in ^{151}Eu and ^{57}Fe experiments, respectively. The SMS experiments were performed during the standard 24-bunch timing mode of the APS with 153 ns separation between the two successive electron bunches for data collection. Avalanche photodiode detectors with time resolution of 1 ns were used for data collection in transmission direction. The SMS spectra were analyzed using the CONUSS

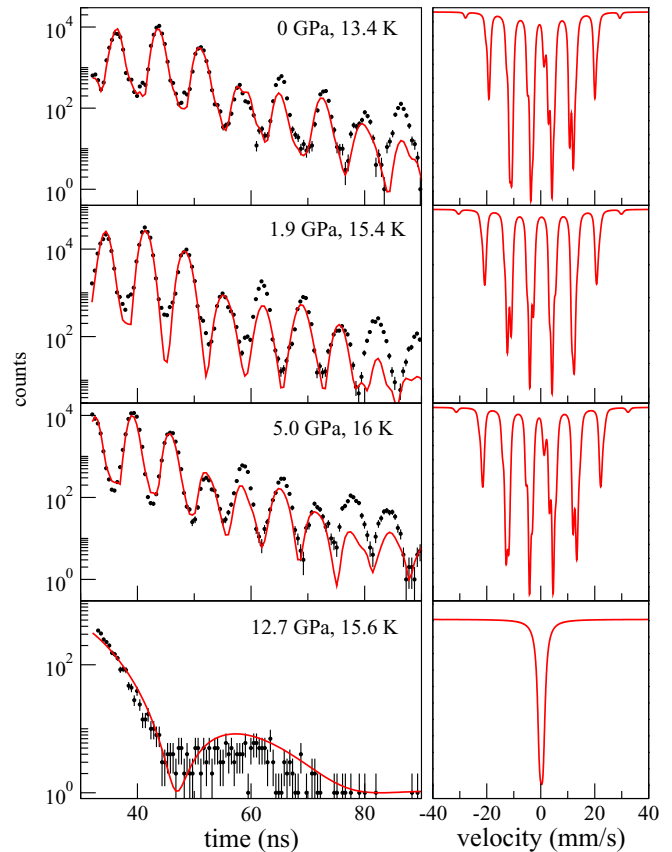


FIG. 1. Selected ^{151}Eu SMS spectra of EuFeAs_2 at high pressures and low temperatures (left panel). The black dots are the experimental data and red lines are fittings obtained using CONUSS program. Corresponding simulated conventional Mössbauer spectra are shown in red lines in the right panel. The IS is set at zero in the simulation.

software [41]. In both ^{151}Eu and ^{57}Fe SMS experiments, the initial pressures were applied at room temperature after neon gas loading, and all subsequent pressures were applied at temperatures of 100 K or lower.

XRD experiments in the parent compound EuFeAs_2 were conducted up to 22 GPa at the 13BM-C beamline (PX²) of the APS, ANL [42]. Polycrystalline sample was ground into fine powder and loaded in a BX-90 DAC with Boehler-Almax anvils of 500 μm culet. Helium was used as pressure medium. Pressures were determined *in situ* from ruby fluorescence. X-rays with a wavelength of 0.434 Å were used. The 2-D diffraction images were integrated using the DIOPTAS software [43]. LeBail refinements on the high pressure XRD data were performed in GSAS-II [44].

III. EXPERIMENTAL RESULTS

A. ^{151}Eu and ^{57}Fe SMS and XRD in EuFeAs_2

SMS in both ^{151}Eu and ^{57}Fe were performed to probe the magnetic transitions in EuFeAs_2 . Typical ^{151}Eu SMS spectra in the time domain along with a theoretical model including magnetic hyperfine field (H_{hf}), quadrupole splitting (QS), texture, and thickness effect are shown in Fig. 1. The corresponding conventional energy-domain Mössbauer spectra

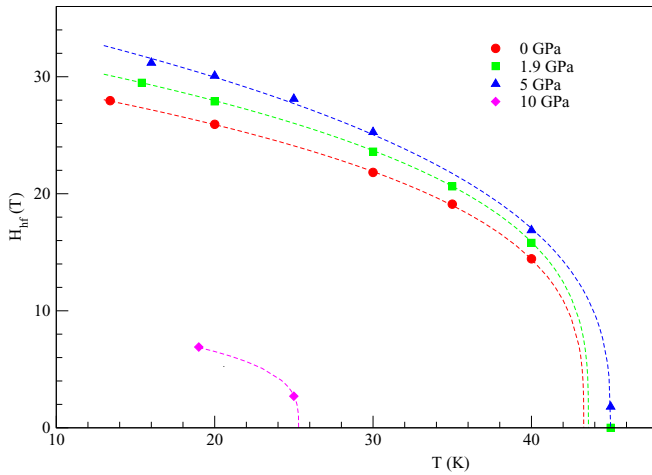


FIG. 2. Magnetic hyperfine fields of ^{151}Eu in EuFeAs_2 as a function of temperature at various pressures. The dashed lines serve as guides to the eye.

are simulated based on the model to illustrate the change of hyperfine field with increasing pressure. The presence of high-frequency quantum beats originating from the magnetic hyperfine field in SMS indicates that EuFeAs_2 is in the magnetic phase. In the magnetic phase, a small QS of less than 2 mm/s was included to fit the SMS data. No sizable QS was observed in the paramagnetic phase. At 12.7 GPa and 15.6 K, the high-frequency beats disappear suddenly, suggesting the absence of local magnetic order, which corresponds to a singlet in conventional Mössbauer spectrum.

The temperature dependence of magnetic hyperfine field [$H_{hf}(T)$] under pressure is plotted in Fig. 2. At ambient pressure the T_N and the saturation magnetic hyperfine field (H_0) of the antiferromagnetically ordered Eu sublattice in EuFeAs_2 are 43.3 K and 31.2 T, respectively, in good agreement with the values from laboratory-based ^{151}Eu Mössbauer measurements at ambient pressure [35]. With increasing pressure to 5 GPa, T_o remains relatively constant. At 10 GPa, T_o decreases abruptly to 25 K. With further increase of pressure to 12.7 GPa, no magnetic order was observed down to 15.6 K. To help understand the sudden collapse of magnetism at 12.7 GPa, the valence state is probed by measuring the IS of Eu ions in EuFeAs_2 . The ^{151}Eu SMS spectra were taken simultaneously from the sample at high pressures and the $\text{Eu}_2\text{O}_3/\text{EuS}$ reference at ambient condition (Fig. 3). The IS of Eu in EuFeAs_2 is -10.82 mm/s at 0 GPa, 300 K, confirming that Eu is in the divalent state. This value is in reasonable agreement with the reported value of -10.56 mm/s [relative to $^{151}\text{Sm}(\text{SmF}_3)$ source] [35]. As shown in the simulated conventional Mössbauer spectra in Fig. 3, IS value moves sluggishly toward the IS value of Eu^{3+} up to 5 GPa. At higher pressure, the IS increases drastically to -1.37 mm/s at 15.3 GPa, suggesting that Eu ions are almost in a trivalent state. The values of hyperfine parameters are tabulated in Table. I. To investigate the pressure effect on the magnetic order in Fe sublattice, ^{57}Fe SMS experiments were carried out at high pressure and low temperature in EuFeAs_2 . Figure 4(a) displays selected ^{57}Fe SMS spectra. The corresponding energy-domain spectra are shown in Fig. 4(b). Fe

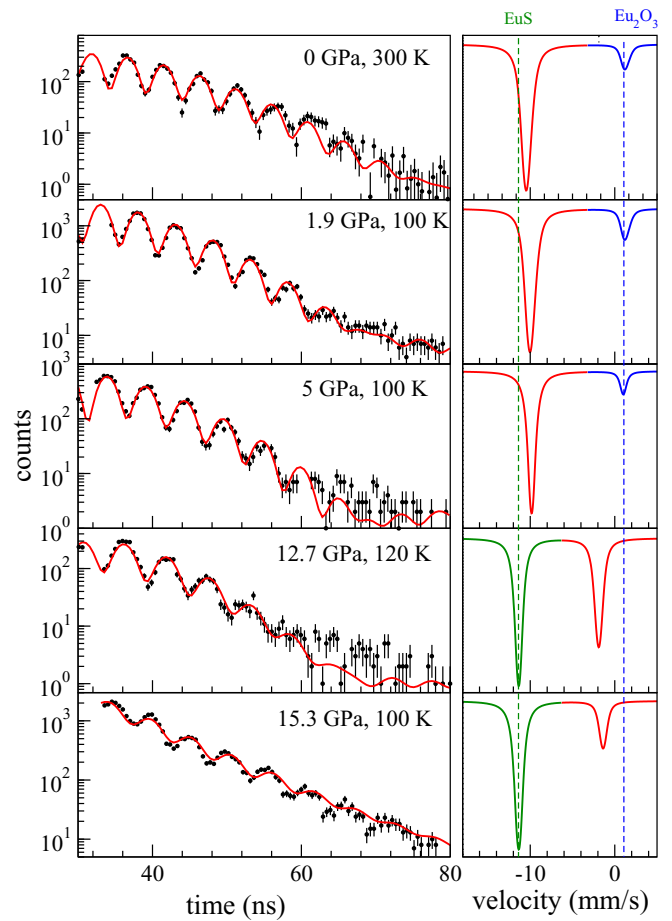


FIG. 3. Left panel: SMS ^{151}Eu spectra in EuFeAs_2 with reference sample under pressure. (right panel) Corresponding simulated spectra in energy domain show the resonant absorption from sample EuFeAs_2 (red) and reference EuS (green) or Eu_2O_3 (blue).

sublattice exhibits a magnetic order up to 8 GPa. At 10 GPa, no magnetic order was observed down to 22.5 K. Extracted H_{hf} values from ^{57}Fe SMS are summarized in Fig. 4(c). SMS data at 0.6 GPa and 28 K give at H_{hf} of 4.5 T, similar to the value of 4.8 T at ambient pressure and 19 K from laboratory-based Mössbauer measurements [35].

Figure 5 shows the selected XRD patterns of EuFeAs_2 under pressures up to 21.8 GPa at room temperature. Due to the low sintering temperature the sample has poor sample crystallinity and weak reflections [34]. Two different ambient structures are reported: Monoclinic structure with a space group of $\text{P}2_1/\text{m}$ [33,34] from polycrystalline samples and orthorhombic structure (space group $\text{Imm}2$) from a single crystal sample with improved crystal growth condition [45]. Similar refinement quality was obtained on the XRD data at 0.1 GPa using both the structure models by the LeBail method. Here orthorhombic structure was adopted to refine the XRD data up to 21.8 GPa (Fig. 5). The unit-cell volume at high pressure is shown in Fig. 6. The volume shows a discontinuity above 10 GPa. Fitting the volume-pressure data with the third-order Birch-Murnaghan equation [46] gives bulk modulus $B_0 = 59.1(2)$ GPa and the pressure derivative $B'_0 = 3.3(1)$ up to 10 GPa and $B_0 =$

TABLE I. List of extracted hyperfine parameters including H_{hf} , QS, and IS of ^{151}Eu in EuFeAs_2 under various pressures and temperatures. The error bars for each parameters are the uncertainties from the refinements.

P (GPa)	T (K)	H_{hf} (T)	QS (mm/s)	IS (mm/s)
0	13.4	27.95(1)	1.24(4)	—
	20	25.93(1)	1.34(3)	—
	30	21.82(2)	1.67(5)	—
	35	19.11(2)	1.20(5)	—
	40	14.44(3)	1.11(6)	—
	60	0	0	—
15.4	300	0	0	-10.82(1)
	15.4	29.48(2)	1.15(5)	—
	20	27.89(1)	1.24(6)	—
	30	23.60(2)	1.29(5)	—
	35	20.63(2)	1.28(7)	—
	40	15.80(3)	0.65(6)	—
1.9	45	0	0	—
	100	0	0	-10.34(1)
	16	31.19(2)	2.0(2)	—
	20	30.08(2)	1.60(9)	—
	25	28.11(3)	1.85(8)	—
	25	25.27(2)	1.90(7)	—
5.0	40	16.88(3)	1.7(1)	—
	45	1.80(2)	0.97(8)	—
	50	0	0	—
	100	0	0	-10.06(2)
10.0	19	6.9(2)	0.7(1)	—
	25	2.70(5)	0.9(2)	—
12.7	15.6	0	0	—
	120	0	0	-1.90(2)
15.3	100	0	0	-1.37(3)

87.1 (2) GPa and $B'_0 = 4.1$ (2) in the higher-pressure region. Figure 7 illustrates the pressure dependence of lattice parameters of EuFeAs_2 obtained from the LeBail refinement of the XRD patterns. An anomaly in the lattice parameters, especially in a , is observed between 10 and 13 GPa. The nature of this anomaly needs to be investigated further with a single crystal sample.

B. SMS in $\text{Eu}(\text{Fe}_{0.96}\text{Ni}_{0.04})\text{As}_2$

As a comparative study of the magnetic phase diagram in EuFeAs_2 , ^{151}Eu SMS experiments were performed in $\text{Eu}(\text{Fe}_{0.96}\text{Ni}_{0.04})\text{As}_2$. Figure 8 presents selected ^{151}Eu SMS spectra at ~ 15 K under pressures at 2.2, 4.8, and 7.5 GPa. At 2.2 GPa and 15.7 K the obtained H_{hf} of $\text{Eu}(\text{Fe}_{0.96}\text{Ni}_{0.04})\text{As}_2$ is 29.5 T, similar to the value in the parent compound EuFeAs_2 at 1.9 GPa and 15.4 K. With pressure application of 7.5 GPa $\text{Eu}(\text{Fe}_{0.96}\text{Ni}_{0.04})\text{As}_2$ no H_{hf} was resolved down to 14.7 GPa, indicating the absence of magnetic order. In the magnetic phase at 2.2 and 4.8 GPa, a small QS of 1–1.8 mm/s has been included to fit the SMS spectra. At 7.5 GPa, 14.7 K no QS was resolved and no H_{hf} was observed down to 14.7 K. The oscillations in the SMS spectrum suggest a minor trivalent impurity phase present in the sample.

The extracted hyperfine field at various pressures and temperatures are shown in Fig. 9. At 2.2 GPa, T_o is 40 K, lower

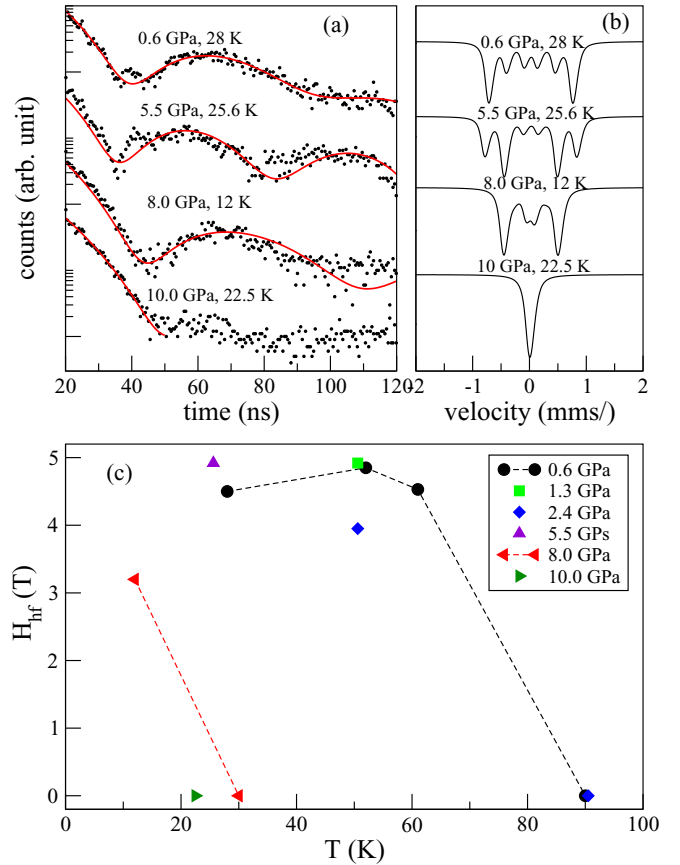


FIG. 4. Selected ^{57}Fe SMS spectra and fits in EuFeAs_2 at high pressures and low temperatures (a) and corresponding simulations in energy domain (b). The IS in simulated spectra is set as zero. The extracted H_{hf} values are shown in (c).

than the value of 43.6 K at 1.9 GPa in EuFeAs_2 . As pressure is increased in $\text{Eu}(\text{Fe}_{0.96}\text{Ni}_{0.04})\text{As}_2$, T_o decreases. At 7.5 GPa, no magnetic order was observed down to 14.7 K. Similar to the parent compound, the IS of Eu ions was measured under

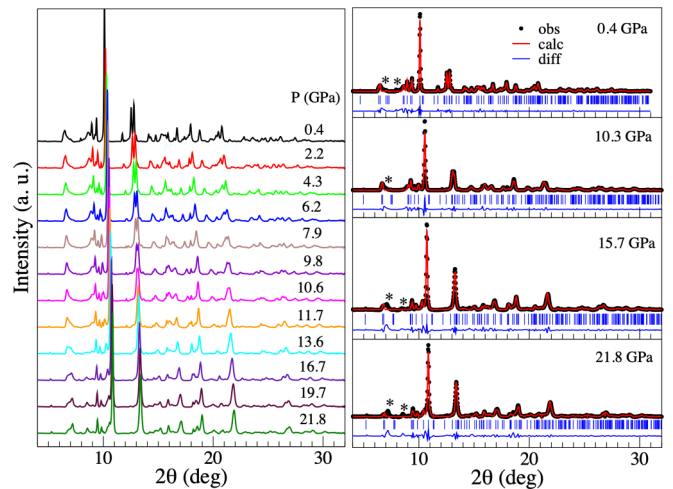


FIG. 5. XRD patterns for EuFeAs_2 at various pressures and room temperature ($\lambda = 0.434$ Å) and LeBail refinements of XRD pattern of EuFeAs_2 at selected pressures. The asterisks indicate the peaks from the minor impurity phase.

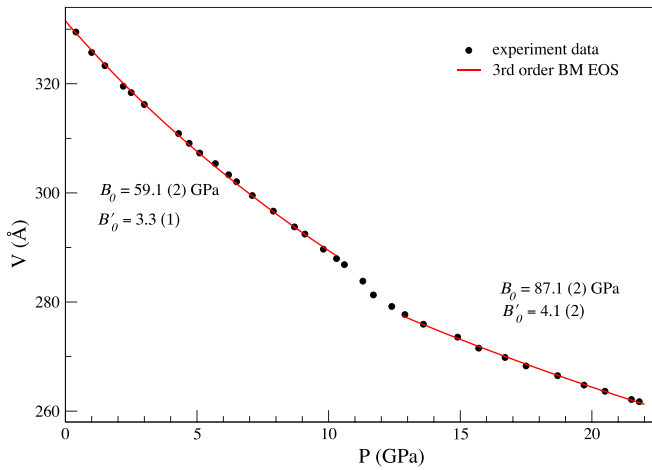


FIG. 6. Unit-cell volume as a function of pressure of EuFeAs_2 . Circles are the experimental data and the red solid lines represent the fit to the third-order Birch-Murnaghan equation. Error bars for the experimental volume are smaller than the symbol size.

pressure with Eu_2O_3 reference. The ^{151}Eu SMS spectra of $\text{Eu}(\text{Fe}_{0.96}\text{Ni}_{0.04})\text{As}_2$ and Eu_2O_3 as well as the simulations in energy domain are shown in Fig. 10. At 1.2 GPa and 300 K, the IS value of Eu in $\text{Eu}(\text{Fe}_{0.96}\text{Ni}_{0.04})\text{As}_2$ is -10.46 mm/s,

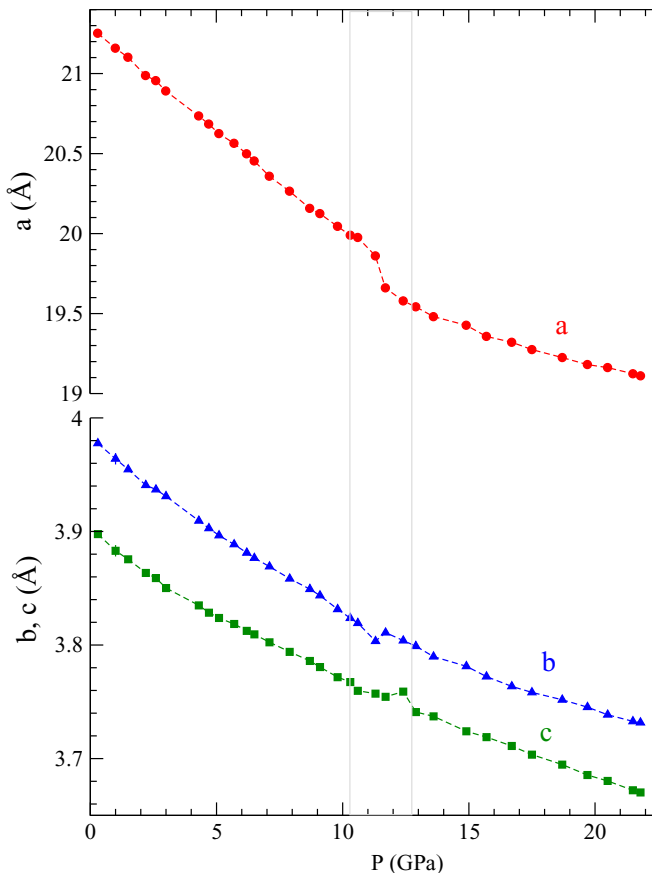


FIG. 7. Pressure dependence of lattice parameters of EuFeAs_2 . An anomaly between 10 and 13 GPa is marked by the gray vertical lines.

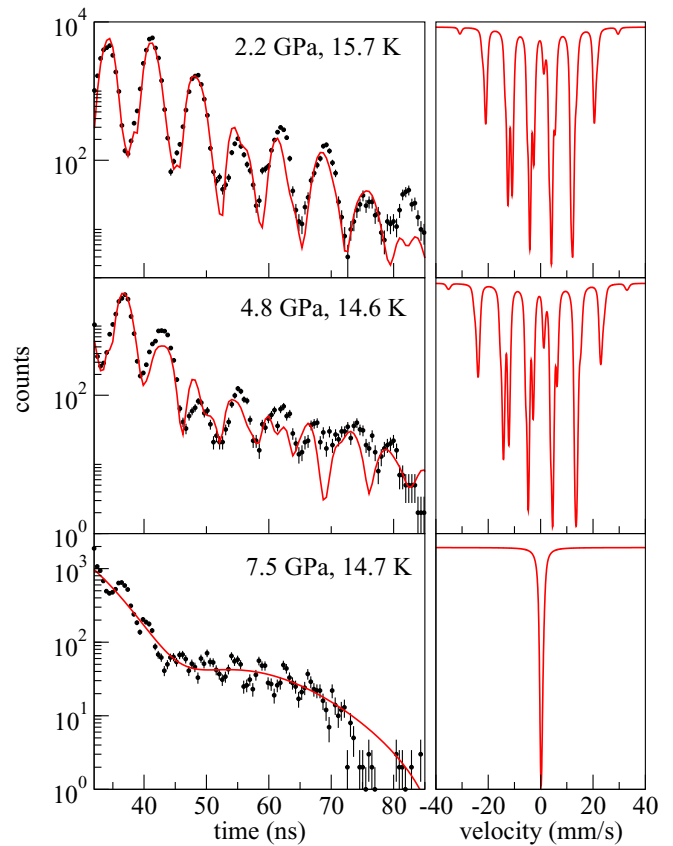


FIG. 8. Representative ^{151}Eu SMS spectra of $\text{Eu}(\text{Fe}_{0.96}\text{Ni}_{0.04})\text{As}_2$ at various pressures and low temperatures (left panel). Simulated conventional laboratory Mössbauer spectra are shown in red lines in the right panel.

indicating Eu is in divalent state. The high-pressure values of the IS in both EuFeAs_2 and $\text{Eu}(\text{Fe}_{0.96}\text{Ni}_{0.04})\text{As}_2$ are summarized in Fig. 11. By assuming that the change in IS comes from the $4f^7$ -to- $4f^6$ transition, the mean valence of Eu ions can be estimated by a simple linear extrapolation shown as the right axis in Fig. 11. IS values of ^{151}Eu in both systems increase continuously with pressure and exhibit similar pressure dependence. The IS values first increase slowly up to 5 GPa and then go up drastically at higher pressure. The valence of Eu increases to ~ 2.9 at 15.3 GPa, 100 K in EuFeAs_2 , and reaches ~ 2.6 at 11.2 GPa, 100 K in $\text{Eu}(\text{Fe}_{0.96}\text{Ni}_{0.04})\text{As}_2$. All the extracted values for hyperfine parameters of the doped compound are summarized in Table II.

IV. DISCUSSION

By combining the experimental results in $\text{Eu}(\text{Fe}_{1-x}\text{Ni}_x)\text{As}_2$ ($x = 0, 0.04$), we have constructed the magnetic P-T phase diagram (Fig. 12). The main observations of the phase diagram are summarized in the following. (i) In EuFeAs_2 the SDW ordering temperature of Fe (T_o^{Fe}) is reduced drastically with applying pressure. By projecting the T_o^{Fe} -P to zero temperature, a full suppression of the SDW order is estimated to occur at ~ 10 GPa. (ii) The magnetic-ordering temperature (T_o^{Eu}) remains almost constant up to 5 GPa and abruptly decreases at higher pressure. At 12.7 GPa, no

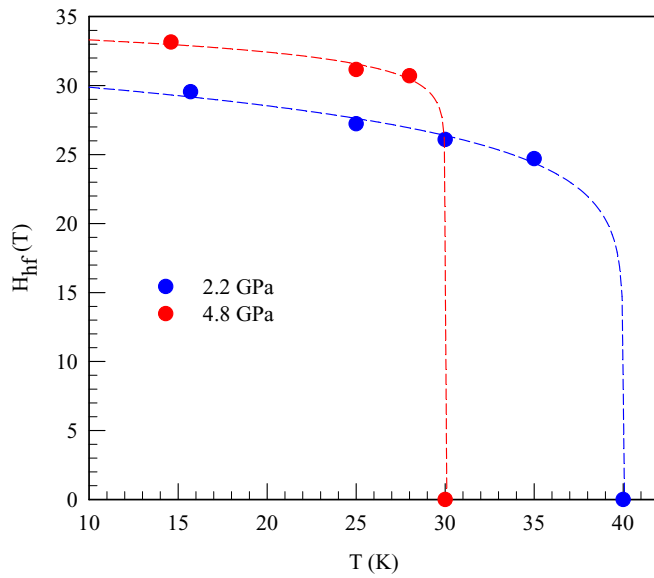


FIG. 9. Magnetic hyperfine field of ^{151}Eu in $\text{Eu}(\text{Fe}_{0.96}\text{Ni}_{0.04})\text{As}_2$ at 2.2 and 4.8 GPa. The dashed lines serve as a guide to the eye.

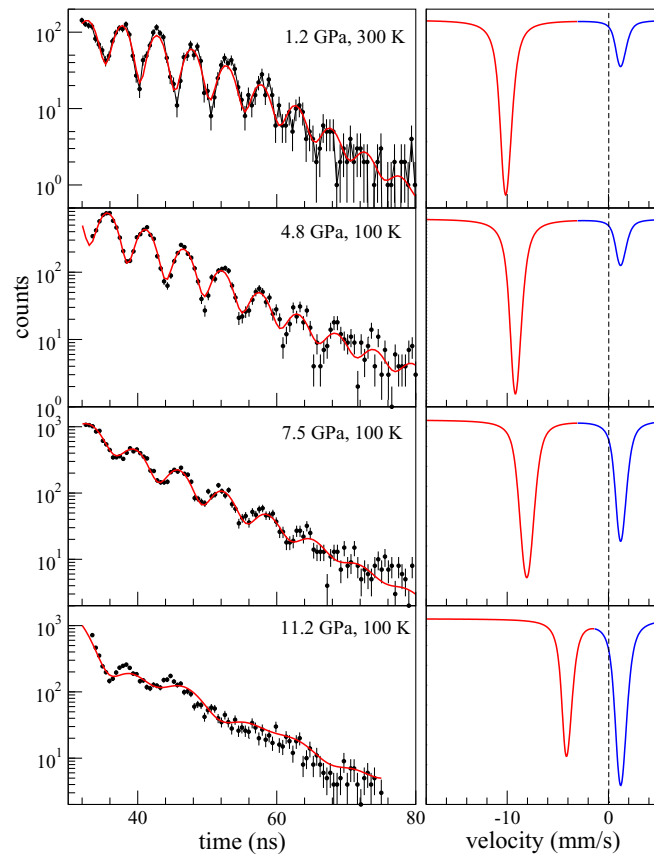


FIG. 10. ^{151}Eu SMS spectra of $\text{Eu}(\text{Fe}_{0.96}\text{Ni}_{0.04})\text{As}_2$ under high pressure and Eu_2O_3 reference in time domain (left panel) and the simulated spectra in energy domain (right panel). In the right panel, red lines are resonant absorption from the $\text{Eu}(\text{Fe}_{0.96}\text{Ni}_{0.04})\text{As}_2$ sample and blue lines represent absorption from Eu_2O_3 . Black dash lines indicate the zero IS.

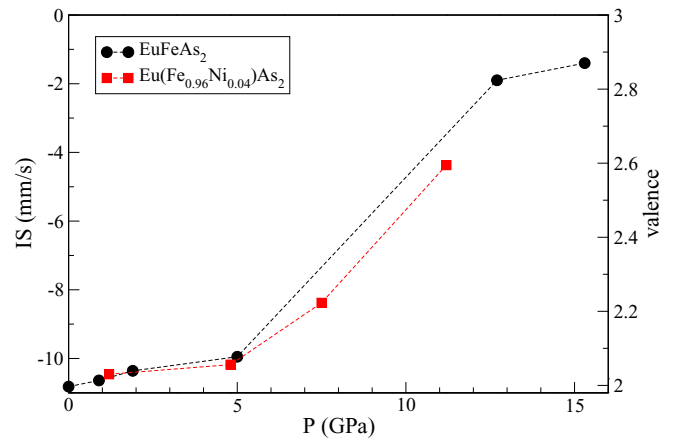


FIG. 11. IS values of ^{151}Eu in EuFeAs_2 and $\text{Eu}(\text{Fe}_{0.96}\text{Ni}_{0.04})\text{As}_2$ at high pressure and various temperatures (left axis) and extrapolated mean valence (right axis).

magnetic order was observed down to 15.6 K. The critical pressure for the local-moment magnetism is estimated to be 11.6 GPa. (iii) The 4% Ni-doping drives the critical pressure (~ 8.2 GPa) to a lower value compared with the parent compound where the local-moment magnetism is fully suppressed.

The high-pressure magnetic and structural behaviors in EuFeAs_2 differ greatly from the 122 and 1144 systems, EuFe_2As_2 and $\text{AEuFe}_4\text{As}_4$ ($A = \text{Rb}, \text{Cs}$). In EuFe_2As_2 the SDW order from itinerant Fe electrons in EuFe_2As_2 is suppressed by pressure and superconductivity occurs in a narrow pressure range of 2.5–3 GPa [24–26,29], while the magnetic-ordering temperature of the Eu sublattice has been found to be insensitive to pressure up to 3.2 GPa. At higher pressure T_N increases and undergoes a transition to a ferromagnetic order around 8 GPa accompanied by the pressure-induced tetragonal to the collapsed-tetragonal phase transition [22,24]. The magnetic order is fully suppressed around 20 GPa, while in $\text{AEuFe}_4\text{As}_4$, the Curie temperature increases monotonically.

TABLE II. List of hyperfine parameters of ^{151}Eu in $\text{Eu}(\text{Fe}_{0.96}\text{Ni}_{0.04})\text{As}_2$. The error bars are the uncertainties in fitting the parameters.

P (GPa)	T (K)	H_{hf} (T)	QS (mm/s)	IS (mm/s)
1.2	300	0	0	-10.46(2)
	15.7	29.53(3)	1.04(4)	—
	25	27.41(4)	0.95(2)	—
2.2	30	26.12(2)	0.70(3)	—
	35	24.43(3)	0.59(3)	—
	40	0	0	—
4.8	14.6	33.26(4)	1.81(6)	—
	25	31.60(3)	1.4(4)	—
	28	30.82(2)	1.0(1)	—
7.5	100	0	0	-9.49(2)
	14.7	0	0	—
	100	0	0	-8.38(2)
11.2	100	0	0	-4.37(2)
	100	0	0	—

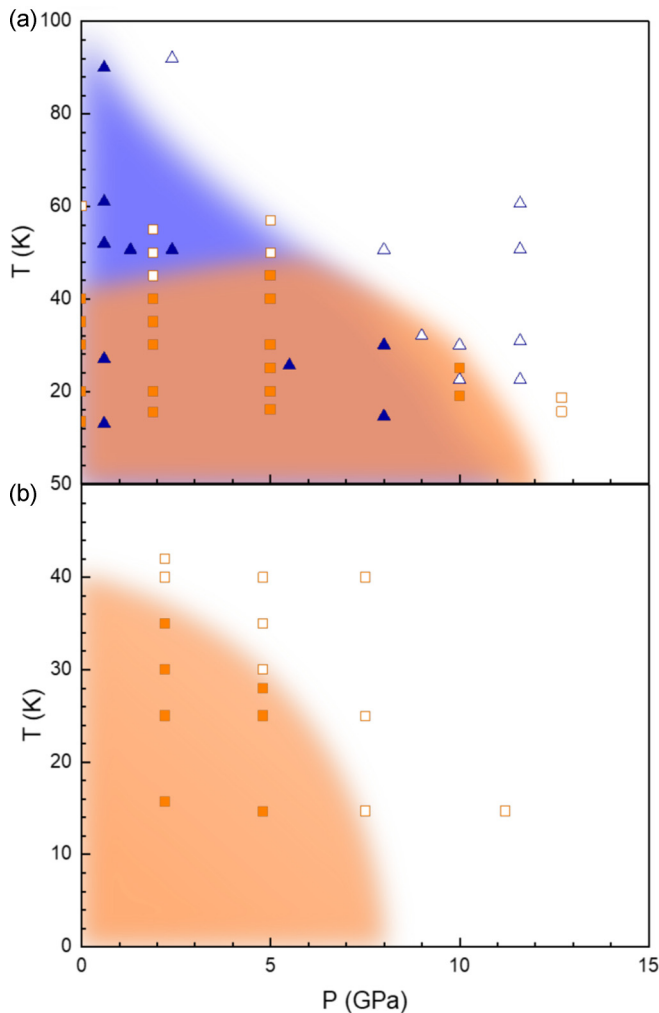


FIG. 12. (a) Schematic P-T phase diagram of EuFeAs_2 . Orange squares represent SMS data in ^{151}Eu and purple triangles indicate ^{57}Fe SMS data of EuFeAs_2 . (b) P-T phase diagram of $\text{Eu}(\text{Fe}_{0.96}\text{Ni}_{0.04})\text{As}_2$. Orange squares show the ^{151}Eu SMS data. Corresponding solid and open symbols differentiate the data in magnetic and paramagnetic phases.

cally up to 30 GPa. In both 122 and 1144 types of pnictides such as EuFe_2As_2 , CaFe_2As_2 , BaFe_2As_2 , and $\text{AEuFe}_4\text{As}_4$, crystal structure transition from tetragonal to either collapsed-tetragonal or half-collapsed-tetragonal driven by pressure has been established [22,31,47]. In EuFeAs_2 an anomaly in lattice parameters and volume occurs above 10 GPa, indicating an isostructure transition possibly related to the suppression of either the SDW order from Fe sublattice or the antiferromagnetic order from Eu ions.

The collapse of local magnetic order in both EuFeAs_2 and $\text{Eu}(\text{Fe}_{0.96}\text{Ni}_{0.04})\text{As}_2$ likely attributes to the drastic valence transition from Eu^{2+} ($4f^7$, $J = 7/2$) to Eu^{3+} ($4f^6$, $J = 0$) (see Fig. 11). In Eu-intermetallic compounds, hybridization of localized $4f$ and conduction electrons contribute to valence transition or intermediate valence [48–51]. In EuFeAs_2 and $\text{Eu}(\text{Fe}_{0.96}\text{Ni}_{0.04})\text{As}_2$ it is possible that the increasing hybridization strength tuned by pressure leads to a weakening

of the magnetic order and eventually the local-moment magnetism collapses at a critical pressure. Electronic structure calculations are needed to provide detailed understanding of the band-structure evolution with pressure. It is noted that in Eu metal the local-moment paramagnetism and superconductivity were found to coexist at pressures above 80 GPa [52].

A similar correlation of magnetic order and valence has been observed in EuFe_2As_2 which experiences a full suppression of magnetic order in Eu ions associated with a significant increase in mean valence [24,53]. On the other hand, in 1144-type $\text{AEuFe}_4\text{As}_4$ ($A = \text{Rb}, \text{Cs}$), pressure greatly enhances the Curie temperature of Eu while it suppresses the superconducting state [31]. It would be interesting to search for pressure-induced superconductivity in EuFeAs_2 and study the high-pressure behavior of superconductivity in $\text{Eu}(\text{Fe}_{0.96}\text{Ni}_{0.04})\text{As}_2$ to compare the interplay of magnetism and superconductivity with the 122 and 1144 systems.

V. CONCLUSION

A microscopic phase diagram in Eu-based iron-pnictide superconductors is the key to understanding the peculiar coexistence of magnetism and superconductivity. To establish the microscopic magnetic P-T phase diagram, we have performed a series of SMS and XRD experiments in $\text{Eu}(\text{Fe}_{1-x}\text{Ni}_x)\text{As}_2$ ($x = 0, 0.04$). An isostructural transition has been observed in EuFeAs_2 above 10 GPa. In the parent compound, the magnetic order of Fe is suppressed by application of pressure at ~ 10 GPa. The local-moment magnetism in Eu ions is expected to be fully suppressed at ~ 11.6 and ~ 8 GPa for EuFeAs_2 and $\text{Eu}(\text{Fe}_{0.96}\text{Ni}_{0.04})\text{As}_2$, respectively. In both systems, the suppression of the local-moment magnetism is associated with a significant increase of the Eu's mean valence. Future experiments exploring the pressure effect on superconductivity are necessary to investigate the interplay of the magnetic ground state with the superconducting state.

ACKNOWLEDGMENTS

We acknowledge the assistance of C. Benson and R. Ferry for the experimental setup at 16ID-D. This research used resources of the APS, a U.S. Department of Energy (DOE) Office of Science User Facility operated for the DOE Office of Science by ANL under Contract No. DE-AC02-06CH11357. This material is based on work supported by the DOE-National Nuclear Security Administration under Award Number DE-NA0003916. Portions of this work were performed at HPCAT (Sector 16), APS, ANL. HPCAT operations are supported by the DOE-NNSA's Office of Experimental Sciences. Support from COMPRES under NSF Cooperative Agreement EAR-1606856 is acknowledged for COMPRES-GSECARS gas-loading system and the PX² program. We thank S. Tkachev for help with the neon and helium loading of the DACs at the APS. G.-H.C. acknowledges the support from the National Key Research and Development Program of China (Grant No. 2016YFA0300202).

- [1] Y. Kamihara, T. Watanabe, M. Hirano, and H. Hosono, *J. Am. Chem. Soc.* **130**, 3296 (2008).
- [2] G. R. Stewart, *Rev. Mod. Phys.* **83**, 1589 (2011).
- [3] F.-C. Hsu, J.-Y. Luo, K.-W. Yeh, T.-K. Chen, T.-W. Huang, P. M. Wu, Y.-C. Lee, Y.-L. Huang, Y.-Y. Chu, D.-C. Yan, and M.-K. Wu, *Proc. Natl. Acad. Sci. USA* **105**, 14262 (2008).
- [4] M. Rotter, M. Tegel, D. Johrendt, I. Schellenberg, W. Hermes, and R. Pöttgen, *Phys. Rev. B* **78**, 020503(R) (2008).
- [5] H. S. Jeevan, D. Kasinathan, H. Rosner, and P. Gegenwart, *Phys. Rev. B* **83**, 054511 (2011).
- [6] A. I. Goldman, D. N. Argyriou, B. Ouladdiaf, T. Chatterji, A. Kreyssig, S. Nandi, N. Ni, S. L. Bud'ko, P. C. Canfield, and R. J. McQueeney, *Phys. Rev. B* **78**, 100506(R) (2008).
- [7] K. Matan, R. Morinaga, K. Iida, and T. J. Sato, *Phys. Rev. B* **79**, 054526 (2009).
- [8] C.-J. Kang, T. Birol, and G. Kotliar, *Phys. Rev. B* **95**, 014511 (2017).
- [9] X. Zhu, F. Han, G. Mu, P. Cheng, B. Shen, B. Zeng, and H.-H. Wen, *Phys. Rev. B* **79**, 220512(R) (2009).
- [10] J. Guo, S. Jin, G. Wang, S. Wang, K. Zhu, T. Zhou, M. He, and X. Chen, *Phys. Rev. B* **82**, 180520(R) (2010).
- [11] S. Kakiya, K. Kudo, Y. Nishikubo, K. Oku, E. Nishibori, H. Sawa, T. Yamamoto, T. Nozaka, and M. Nohara, *J. Phys. Soc. Jpn.* **80**, 093704 (2011).
- [12] A. Iyo, K. Kawashima, T. Kinjo, T. Nishio, S. Ishida, H. Fujihisa, Y. Gotoh, K. Kihou, H. Eisaki, and Y. Yoshida, *J. Am. Chem. Soc.* **138**, 3410 (2016).
- [13] S. Zapf and M. Dressel, *Rep. Prog. Phys.* **80**, 016501 (2017).
- [14] H. S. Jeevan, Z. Hossain, D. Kasinathan, H. Rosner, C. Geibel, and P. Gegenwart, *Phys. Rev. B* **78**, 052502 (2008).
- [15] S. Nandi, W. T. Jin, Y. Xiao, Y. Su, S. Price, D. K. Shukla, J. Strempper, H. S. Jeevan, P. Gegenwart, and T. Brückel, *Phys. Rev. B* **89**, 014512 (2014).
- [16] H. S. Jeevan, Z. Hossain, D. Kasinathan, H. Rosner, C. Geibel, and P. Gegenwart, *Phys. Rev. B* **78**, 092406 (2008).
- [17] Z. Ren, Z. Zhu, S. Jiang, X. Xu, Q. Tao, C. Wang, C. Feng, G. Cao, and Z. Xu, *Phys. Rev. B* **78**, 052501 (2008).
- [18] Z. Ren, Q. Tao, S. Jiang, C. Feng, C. Wang, J. Dai, G. Cao, and Z. Xu, *Phys. Rev. Lett.* **102**, 137002 (2009).
- [19] Y. Liu, Y.-B. Liu, Z.-T. Tang, H. Jiang, Z.-C. Wang, A. Ablimit, W.-H. Jiao, Q. Tao, C.-M. Feng, Z.-A. Xu, and G.-H. Cao, *Phys. Rev. B* **93**, 214503 (2016).
- [20] K. Kawashima, T. Kinjo, T. Nishio, S. Ishida, H. Fujihisa, Y. Gotoh, K. Kihou, H. Eisaki, Y. Yoshida, and A. Iyo, *J. Phys. Soc. Jpn.* **85**, 064710 (2016).
- [21] W. Uhoya, G. Tsoi, Y. K. Vohra, M. A. McGuire, A. S. Sefat, B. C. Sales, D. Mandrus, and S. T. Weir, *J. Phys.: Condens. Matter* **22**, 292202 (2010).
- [22] W. O. Uhoya, G. M. Tsoi, Y. K. Vohra, M. A. McGuire, and A. S. Sefat, *J. Phys.: Condens. Matter* **23**, 365703 (2011).
- [23] Y. Tokiwa, S.-H. Hübner, O. Beck, H. S. Jeevan, and P. Gegenwart, *Phys. Rev. B* **86**, 220505(R) (2012).
- [24] K. Matsubayashi, K. Munakata, M. Isobe, N. Katayama, K. Ohgushi, Y. Ueda, N. Kawamura, M. Mizumaki, N. Ishimatsu, M. Hedo, I. Umehara, and Y. Uwatoko, *Phys. Rev. B* **84**, 024502 (2011).
- [25] W. T. Jin, Y. Xiao, S. Nandi, S. Price, Y. Su, K. Schmalzl, W. Schmidt, T. Chatterji, A. Thamizhavel, and T. Brückel, *Phys. Rev. B* **100**, 014503 (2019).
- [26] N. Kurita, M. Kimata, K. Kodama, A. Harada, M. Tomita, H. S. Suzuki, T. Matsumoto, K. Murata, S. Uji, and T. Terashima, *Phys. Rev. B* **83**, 214513 (2011).
- [27] C. F. Miclea, M. Nicklas, H. S. Jeevan, D. Kasinathan, Z. Hossain, H. Rosner, P. Gegenwart, C. Geibel, and F. Steglich, *Phys. Rev. B* **79**, 212509 (2009).
- [28] T. Terashima, M. Kimata, H. Satsukawa, A. Harada, K. Hazama, S. Uji, H. S. Suzuki, T. Matsumoto, and K. Murata, *J. Phys. Soc. Jpn.* **78**, 083701 (2009).
- [29] S. Ikeda, Y. Tsuchiya, X.-W. Zhang, S. Kishimoto, T. Kikegawa, Y. Yoda, H. Nakamura, M. Machida, J. K. Glasbrenner, and H. Kobayashi, *Phys. Rev. B* **98**, 100502(R) (2018).
- [30] Y. Liu, Y. B. Liu, Q. Chen, Z. T. Tang, W. H. Jiao, Q. Tao, Z. A. Xu, and G. H. Cao, *Sci. Bull.* **61**, 1213 (2016).
- [31] D. E. Jackson, D. VanGennep, W. Bi, D. Zhang, P. Materne, Y. Liu, G.-H. Cao, S. T. Weir, Y. K. Vohra, and J. J. Hamlin, *Phys. Rev. B* **98**, 014518 (2018).
- [32] L. Xiang, S. L. Bud'ko, J.-K. Bao, D. Y. Chung, M. G. Kanatzidis, and P. C. Canfield, *Phys. Rev. B* **99**, 144509 (2019).
- [33] J. Yu, T. Liu, B. J. Pan, B. B. Ruan, X. C. Wang, Q. G. Mu, K. Zhao, G. F. Chen, and Z. A. Ren, *Sci. Bull.* **62**, 218 (2017).
- [34] Y. Liu, Y. Liu, W. Jiao, Z. Ren, and G. Cao, *Sci. China Phys. Mech. Astron.* **61**, 127405 (2018).
- [35] M. A. Albedah, Z. M. Stadnik, O. Fedoryk, Y.-b. Liu, and G.-h. Cao, *J. Magn. Magn. Mater.* **503**, 166603 (2020).
- [36] J. Y. Zhao, W. Bi, S. Sinogeikin, M. Y. Hu, E. E. Alp, X. C. Wang, C. Q. Jin, and J. F. Lin, *Rev. Sci. Instrum.* **88**, 125109 (2017).
- [37] S. V. Sinogeikin, J. S. Smith, E. Rod, C. Lin, C. Kenney-Benson, and G. Shen, *Rev. Sci. Instrum.* **86**, 072209 (2015).
- [38] A. D. Chijioke, W. J. Nellis, A. Soldatov, and I. F. Silvera, *J. Appl. Phys.* **98**, 114905 (2005).
- [39] J. G. Stevens, *Hyperfine Interact.* **13**, 221 (1983).
- [40] W. Bi, N. M. Souza-Neto, D. Haskel, G. Fabbris, E. E. Alp, J. Zhao, R. G. Hennig, M. M. Abd-Elmeguid, Y. Meng, R. W. McCallum, K. Dennis, and J. S. Schilling, *Phys. Rev. B* **85**, 205134 (2012).
- [41] W. Sturhahn, *Hyperfine Interact.* **125**, 149 (2000).
- [42] D. Zhang, P. K. Dera, P. J. Eng, J. E. Stubbs, J. S. Zhang, V. B. Prakapenka, and M. L. Rivers, *J. Vis. Exp.* **16**, 54660 (2017).
- [43] C. Prescher and V. B. Prakapenka, *High Press. Res.* **35**, 223 (2015).
- [44] B. H. Toby and R. B. Von Dreele, *J. Appl. Crystallogr.* **46**, 544 (2013).
- [45] J. Yu, T. Liu, K. Zhao, B.-J. Pan, Q.-G. Mu, B.-B. Ruan, and Z.-A. Ren, *Acta Phys. Sin.* **67**, 207403 (2018).
- [46] F. Birch, *J. Geophys. Res.* **83**, 1257 (1978).
- [47] R. Mittal, S. K. Mishra, S. L. Chaplot, S. V. Ovsyannikov, E. Greenberg, D. M. Trots, L. Dubrovinsky, Y. Su, T. Brueckel, S. Matsuishi, H. Hosono, and G. Garbarino, *Phys. Rev. B* **83**, 054503 (2011).
- [48] Z. Hossain, C. Geibel, N. Senthikumar, M. Deppe, M. Baenitz, F. Schiller, and S. L. Molodtsov, *Phys. Rev. B* **69**, 014422 (2004).
- [49] H.-F. Zhai, Z.-T. Tang, H. Jiang, K. Xu, K. Zhang, P. Zhang, J.-K. Bao, Y.-L. Sun, W.-H. Jiao, I. Nowik, I. Felner, Y.-K. Li, X.-F. Xu, Q. Tao, C.-M. Feng, Z.-A. Xu, and G.-H. Cao, *Phys. Rev. B* **90**, 064518 (2014).
- [50] K. S. Nemkovski, D. P. Kozlenko, P. A. Alekseev, J.-M. Mignot, A. P. Menushenkov, A. A. Yaroslavl'tsev, E. S. Clementyev,

- A. S. Ivanov, S. Rols, B. Klobes, R. P. Hermann, and A. V. Gribanov, *Phys. Rev. B* **94**, 195101 (2016).
- [51] S. A. Medvedev, P. Naumov, O. Barkalov, C. Shekhar, T. Palasyuk, V. Ksenofontov, G. Wortmann, and C. Felser, *J. Phys.: Condens. Matter* **26**, 335701 (2014).
- [52] W. Bi, J. Lim, G. Fabbris, J. Zhao, D. Haskel, E. E. Alp, M. Y. Hu, P. Chow, Y. Xiao, W. Xu, and J. S. Schilling, *Phys. Rev. B* **93**, 184424 (2016).
- [53] R. S. Kumar, Y. Zhang, A. Thamizhavel, a. Svane, G. Vaitheeswaran, V. Kanchana, Y. Xiao, P. Chow, C. Chen, and Y. Zhao, *Appl. Phys. Lett.* **104**, 042601 (2014).